THE UNIVERSITY OF ALABAMA® | University Libraries

Photodissociation of Water and $O(^3P_J)$ Formation on a Lunar Impact Melt Breccia

Alice DeSimone – Georgia Institute of Technology
Thomas M. Orlando – Georgia Institute of Technology

Deposited 10/23/2018

Citation of published version:
DeSimone, A., Orland, T. (2014): Photodissociation of Water and $O(^3P_J)$ Formation on a Lunar Impact Melt Breccia. *Journal of Geophysical Research*, 119(4).
DOI: https://doi.org/10.1002/2013JE004598

© 2014. American Geophysical Union. All Rights Reserved.

AGU PUBLICATIONS

JGR

Journal of Geophysical Research: Planets

RESEARCH ARTICLE
10.1002/2013JE004598

This article is a companion to *DeSimone and Orlando* [2014] doi:10.1002/2013JE004599.

Key Points:
- 157-nm photons dissociate water on a lunar impact melt breccia
- Recombination and photodissociation of hydroxyl radicals form O(3P)
- Cross sections representing rates of surface hydroxyl depletion were calculated

Correspondence to:
T. M. Orlando,
thomas.orlando@chemistry.gatech.edu

Citation:
DeSimone, A. J., and T. M. Orlando (2014), Photodissociation of water and $O(^3P_J)$ formation on a lunar impact melt breccia, *J. Geophys. Res. Planets*, *119*, 894–904, doi:10.1002/2013JE004598.

Received 19 DEC 2013
Accepted 25 MAR 2014
Accepted article online 28 MAR 2014
Published online 30 APR 2014

Photodissociation of water and $O(^3P_J)$ formation on a lunar impact melt breccia

Alice J. DeSimone[1] and Thomas M. Orlando[1,2]

[1]School of Chemistry and Biochemistry, Georgia Institute of Technology, Atlanta, Georgia, USA, [2]School of Physics, Georgia Institute of Technology, Atlanta, Georgia, USA

Abstract Photodissociation of water deposited on an impact melt breccia collected during Apollo 16 was studied by measuring $O(^3P_{J\,=\,2,1,0})$ photoproducts detected with resonance-enhanced multiphoton ionization. For each spin-orbit state, the oxygen atom time-of-flight (TOF) spectrum was measured as a function of H_2O exposure and 157 nm irradiation time. Four Maxwell-Boltzmann distributions with translational temperatures of 10,000 K, 1800 K, 400 K, and 102 K were required to fit the data. The most likely formation mechanisms are molecular hydrogen elimination following ion-electron recombination, secondary recombination of hydroxyl radicals, and photodissociation of adsorbed hydroxyls. The irradiation time required to reach maximum oxygen signal suggests that water clusters into islands when adsorbing on the lunar impact melt breccia. After enough irradiation for the oxygen atom yield to reach its maximum, the slowly decreasing signal was fit with an exponential curve to obtain a cross section that represents the rate of surface hydroxyl depletion. For 0.1, 1, and 5 Langmuir ($1\,L = 10^{-6}$ Torr s) H_2O exposure, respectively, the measured $O(^3P)$ depletion cross sections were 4.9×10^{-20}, 6.6×10^{-20}, and 4.6×10^{-20} cm^2. These results imply that photodissociation of water on the lunar surface cannot account for the large mass-16 (±1 amu) signal observed in the lunar atmosphere. Unless another significant source of oxygen atoms is present, this unexpectedly large signal is likely due to CH_4 or OH.

1. Introduction

The measurement of oxygen in the Moon's atmosphere has been a priority of lunar scientists for many years. In 1973, scientists analyzing data from the Apollo 17 UV spectrometer placed an upper limit of 80 cm^{-3} on the concentration of atmospheric oxygen atoms near the lunar surface [*Fastie et al.*, 1973]. In 1991, reanalysis of the same data resulted in an upper limit of 500 cm^{-3} [*Feldman and Morrison*, 1991]. Most recently, pickup ion observations indicated large neutral abundances at mass 16, indicating a new upper limit for the density of oxygen atoms: 12,000 cm^{-3}, more than 20 times the previous optical limit [*Halekas et al.*, 2013]. This recent study also noted that some oxygen atoms were thermally equilibrated to the surface temperature, which would be surprising if they were ejected by solar wind-ion sputtering [*Halekas et al.*, 2013]. Perhaps these unanticipated oxygen concentrations are not only due to sputtering but also to recombination reactions of hydroxyls formed by photodissociation of water.

Several studies support the presence of water on the Moon with infrared (IR) absorption data showing broad 3 μm hydration features [*Clark*, 2009; *Pieters et al.*, 2009; *Sunshine et al.*, 2009]. The IR data show maximum absorption at 2.8 μm, indicating stretching vibrations of hydroxyls, and less intense absorptions at wavelengths greater than 3.0 μm that may be attributed to H_2O. Additionally, laboratory temperature-programmed desorption experiments imply that OH is more likely to be present than H_2O in sunlit lunar regions [*Hibbitts et al.*, 2011; *Poston et al.*, 2013].

Vacuum ultraviolet irradiation of amorphous solid water (ASW) plays a crucial role in both interstellar and planetary chemistry [*Cassidy et al.*, 2010; *Thiel and Madey*, 1987], so this process has been studied extensively [*Andersson et al.*, 2011; *DeSimone et al.*, 2013; *Hama et al.*, 2009; *Hama et al.*, 2010; *Nishi et al.*, 1984; *Yabushita et al.*, 2008; *Yabushita et al.*, 2009]. In particular, we recently measured formation of the ground-state oxygen fragment, $O(^3P_J)$, by 157 nm irradiation of ASW on an oxide-coated copper surface and concluded that the most likely mechanisms of $O(^3P_J)$ formation are molecular elimination after ion-electron recombination, secondary recombination of hydroxyl radicals, and photodissociation of adsorbed hydroxyls [*DeSimone and Orlando*, 2014b]. In the present work, $O(^3P_J)$ produced by 157 nm irradiation of ASW has been measured as a function of spin-orbit (J) state, H_2O exposure, and irradiation time using a genuine lunar impact melt breccia

©2014. American Geophysical Union. All Rights Reserved.

as the substrate. Along with our complementary study of H_2O desorption by 157 nm irradiation of ASW on the impact melt breccia [*DeSimone and Orlando*, 2014a], this work investigates the competition between photodesorption and photodissociation of water on a lunar surface.

2. Experiments and Data Analysis

2.1. Laboratory Measurements

The ultrahigh vacuum (UHV) chamber utilized in all experiments has been described previously [*DeSimone et al.*, 2013]. Its key components are a time-of-flight (TOF) mass spectrometer and a leak valve for dosing small quantities of water vapor. The chamber's base pressure was 2×10^{-10} Torr, and background dosing of H_2O was typically performed at 1–5 $\times$ 10^{-8} Torr. H_2O exposure in Langmuir (1 L = 10^{-6} Torr s) was estimated by multiplying the chamber pressure during dosing by the time spent at that elevated pressure. If every water molecule hitting the cold sample sticks to it, 1 L H_2O exposure leads to a thin film of ASW with single-molecule thickness, though in reality clusters are likely to form. In this paper, 1 L ASW refers to the ice coverage resulting from a dose of 1 L H_2O. Experiments were generally performed at the minimum sample temperature of 102 K. The lunar substrate was an impact melt breccia collected during Apollo 16 (NASA sample 60017.196), cut to be flat on one side. The flat side was attached tightly to the sample holder by tantalum strips in order to maximize cooling efficiency.

The experimental procedure, which has been more thoroughly described in our previous work [*DeSimone and Orlando*, 2014b], involves two lasers in a pump-probe setup. First, the pump laser causes dissociation and/or desorption. Then, the probe laser resonantly ionizes specific neutral products in a process called resonance-enhanced multiphoton ionization (REMPI). Varying the time delay between the two lasers allows the velocity distributions of neutral dissociation products to be determined.

An excimer laser (GAM Laser, EX5) produced 157 nm photons, which entered the UHV chamber through a MgF_2 window after passing through a small tube purged with nitrogen gas. The excimer laser energy was typically 150–350 μJ cm^{-2} per pulse. $O(^3P_{J=2,1,0})$ photoproducts were detected with 2 + 1 REMPI at wavelengths between 225.6 and 226.4 nm [*Matsumi et al.*, 1991], which were obtained by frequency doubling the visible output of a Nd: YAG-pumped optical parametric oscillator (Spectra-Physics, MOPO-SL). The REMPI laser beam was focused down to a volume of ~10 μm^3. The distance between the surface and the detection region based on laser alignment was 3 ± 0.5 mm, but a more precise value of 3.4 mm was determined by fitting the thermal component of several TOF spectra with Maxwell-Boltzmann distributions corresponding to 102 K.

To probe different parts of the desorption plume, the time between the desorption and ionization laser pulses was varied with a delay generator from 0 to 50 μs. The flight time of the neutral oxygen atom from the surface to the focal point of the ionization laser equals the delay time between the two lasers. In order to determine the TOF spectrum of the O-atom desorbate, at each delay time the oxygen peak in the mass spectrum was integrated to obtain the total signal intensity. The spatial and temporal alignment of the two lasers is shown in the first figure of our companion paper [*DeSimone and Orlando*, 2014a].

2.2. Simulation of TOF Spectra and Velocity Distributions

As discussed in the companion paper, a sum of flux-weighted Maxwell-Boltzmann distributions was used to simulate the TOF spectra [*Zimmermann and Ho*, 1995]. Four Maxwell-Boltzmann components, $S(t, T_{trans})$, were required to adequately fit the experimental data:

$$S(t, T_{trans}) = At^{-4} \exp\left(\frac{-mr^2}{2k_B T_{trans} t^2}\right), \quad (1)$$

where T_{trans} is the translational temperature, r is the distance between the surface and the detection region, and A is a scaling factor.

$O(^3P_J)$ data were also plotted in velocity space using the Jacobian transform, $P_v(v) = tr^2 S(t)$, where $v = r/t$ and $S(t)$ is the measured signal intensity at each time. Velocity distributions were fit with four Maxwell-Boltzmann components of the form:

$$P_v(v, T_{trans}) = Av^3 \exp\left(\frac{-mv^2}{2k_B T_{trans}}\right), \quad (2)$$

where the values of T_{trans} were those used to fit the TOF spectra.

©2014. American Geophysical Union. All Rights Reserved.

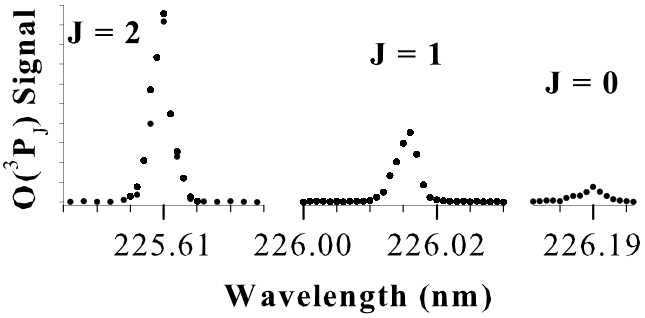

Figure 1. REMPI spectrum for $O(^3P_J)$ produced by 157 nm irradiation of 1 L ASW on the lunar slab at 102 K.

3. Results

Figure 1 shows a representative REMPI spectrum for the detection of $O(^3P_J)$ due to 157 nm irradiation of 1 L ASW on the lunar slab with TOF = 1.7 μs. Wavelengths shown in Figure 1 are in air, and the corresponding vacuum wavelengths can be found by adding ~0.06 nm. The relative peak areas are 9.9, 4.2, and 1 for $J = 2$, 1, and 0, respectively.

As shown in Figure 2, the shape of the TOF spectrum was dependent on spin-orbit (J) state. Consequently, a useful spin-orbit temperature could not be calculated based on the peak area ratios in Figure 1, which are only true at a single flight time. Only by integrating the entire TOF spectrum and its components could valid spin-orbit temperatures be obtained.

Figure 2 also shows that the slow component of the TOF spectrum from 5 L ASW is much larger for $J = 2$ than for $J = 1$ or 0. Figure 3 shows that both the slowest and fastest components disproportionately increased with coverage for $J = 2$. TOF spectra were also measured for $J = 1$ and $J = 0$ at 0.1, 1, 5, and 50 L. All of these TOF spectra were fit with a sum of up to four Maxwell-Boltzmann components with translational temperatures of 10,000 K, 1600–2000 K, 400 K, and the surface temperature (102 K). These are the same translational temperatures that were used to describe the TOF spectra for $O(^3P_J)$ from thick ASW [*DeSimone and Orlando*, 2014b], although the relative intensities of these components differ.

A subthermal, non-Maxwellian component was also observed in some scans, and this signal that exceeded the sum of the four Maxwell-Boltzmann distributions at long flight times was referred to as the diffusion component. Figure 4 shows the $O(^3P_2)$ TOF spectrum for 50 L H_2O exposure, the four Maxwell-Boltzmann components, and the sum of those components. The error bars represent 95% confidence intervals calculated from 16 back-to-back scans after substantial irradiation. Although Figure 4 only shows data up to 30 μs, signal was collected out to 50 μs to capture the entire diffusion component. Figure 5 shows the corresponding velocity distribution for $O(^3P_2)$ desorbing from 50 L ASW on the lunar slab.

In order to pinpoint the distance between the surface and the detection region (r), the thermal component of the velocity distribution needs to be fit accurately. In simulating the velocity distribution of $O(^3P_2)$ from 1 L ASW on the lunar slab (Figure 6), the 102 K component fits best with $r = 3.4$ mm. Thus, this flight distance was used for all fits. The most common velocities for $O(^3P_2)$ produced by 157 nm irradiation of 1 L ASW on the lunar slab were 450–950 m/s. For 50 L ASW (Figure 5), the most common velocities were lower (~370 m/s) due to the large diffusion component. The peak velocities for the four Maxwell-Boltzmann components were 400, 800, 1700, and 4000 m/s.

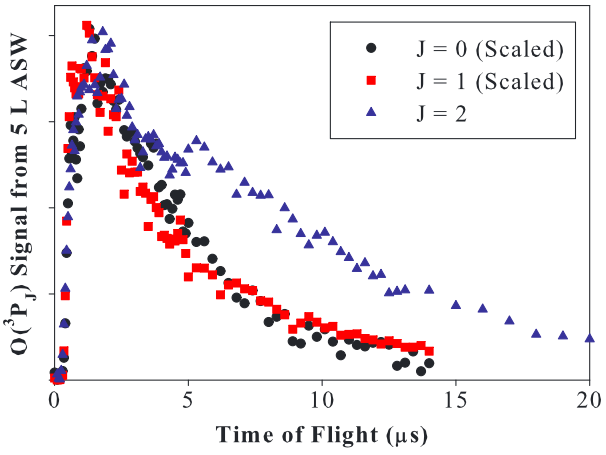

Figure 2. TOF spectra for $O(^3P_J)$ produced by 157 nm irradiation of 5 L ASW on the lunar slab at 102 K.

Table 1 summarizes the relative yields and component areas for each J state at each exposure. The rows labeled "Background" show the percentage of the total TOF area attributed to each Maxwell-Boltzmann component for scans performed without any intentional dosing of water. Note that "0.1 L" should be interpreted as 0.1 L plus a small amount of water deposited during cooling, which could not be quantified because irradiation during cooling was used to keep the surface free of contaminants.

©2014. American Geophysical Union. All Rights Reserved.

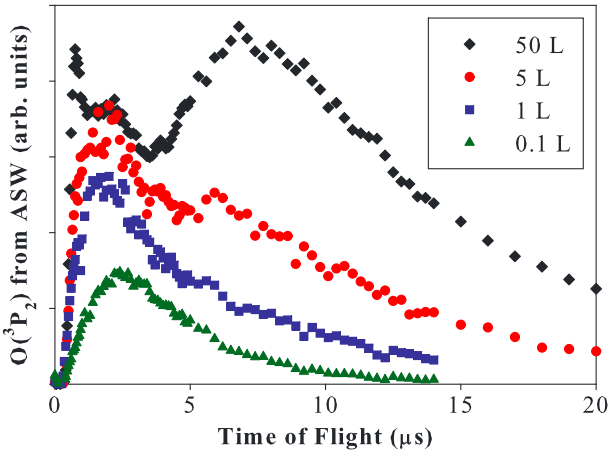

Figure 3. TOF spectra for $O(^3P_2)$ produced by 157 nm irradiation of 0.1, 1, 5, and 50 L ASW on the lunar slab at 102 K.

The velocity distribution of $O(^3P_2)$ measured before any intentional dosing on the impact melt breccia was nearly identical to the corresponding background velocity distribution on the copper sample mount (Figure 7), so this signal was attributed to deposition of water from the UHV chamber's background rather than to oxygen intrinsic to the lunar material. It is not surprising that the rising edges of the velocity distributions in Figure 7 do not perfectly overlap because the copper was 20 K colder than the impact melt breccia.

Notice that the last row of Table 1 contains information about 50 L ASW at 140 K. Diffusion should be greatly enhanced by heat, and the diffusion component did indeed increase from 50.7% to 62.6% of the total signal, even as the total yield dropped due to thermal desorption. Three components increased in magnitude with increasing coverage: 10,000 K, 102 K, and diffusion. The 1800 K and 400 K components appeared in every scan, but their magnitudes did not increase nearly as much as the other components with increasing ASW coverage.

Table 2 shows the Boltzmann temperatures of the spin-orbit levels, $T_{spin\text{-}orbit}$, associated with each TOF component and the overall yields for each exposure. The 0.1 L row nicely illustrates the trend for components with higher translational temperatures to also have higher spin-orbit temperatures. Several of the calculated temperatures were negative, indicating even more excited oxygen atoms than for large positive spin-orbit temperatures. The average overall spin-orbit temperature was 524 K, quite similar to the 543 K average spin-orbit temperature on the copper sample holder [*DeSimone and Orlando*, 2014b].

The TOF spectra summarized in Table 1 were measured after the initial period of irradiation during which signal increased dramatically, as shown in Figure 8. The $O(^3P_2)$ signal increased with similar rates for both the 10,000 K component (TOF = 0.6 μs) and the 102 K component (TOF = 7.0 μs) for 50 L ASW on the impact melt breccia.

While the irradiation time to reach maximum signal was only about 4 min (~ 5×10^{17} photons cm^{-2}) for 50 L ASW, it took much longer for signals from 0.1 to 5 L ASW to stabilize. Figure 9 shows the effect of increasing irradiation on $O(^3P_2)$ signal from 0.1 L ASW. With increasing irradiation, the 400 K component increased while other components remained the same size, causing the peak maximum to shift to slightly longer times. After about 45 min of irradiation, the peak area started to decrease slowly. Several hours of irradiation did not make the signal disappear entirely, since the rate of background H_2O deposition eventually became comparable to the rate of $O(^3P)$ depletion. For higher coverages, the 400 K component is harder to pinpoint due to the increasing number and magnitude of other peaks.

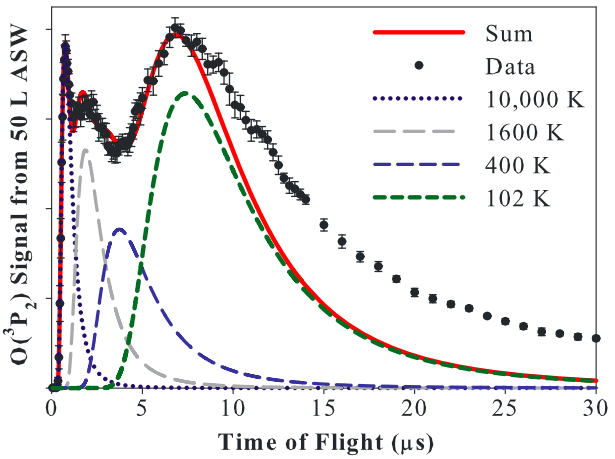

Figure 4. TOF spectrum for $O(^3P_2)$ produced by long-term 157 nm irradiation of 50 L ASW on the lunar slab at 102 K. The sum of four Maxwell-Boltzmann components fits the data well until about 8 μs. The remaining subthermal signal was not fit by a Maxwell-Boltzmann distribution.

Figure 10 shows the effect of increasing irradiation on the $O(^3P_2)$ signal for 5 L ASW. Maximum total integrated signal was reached after irradiation with ~ 5×10^{18} photons cm^{-2} (75 min). However, the

©2014. American Geophysical Union. All Rights Reserved.

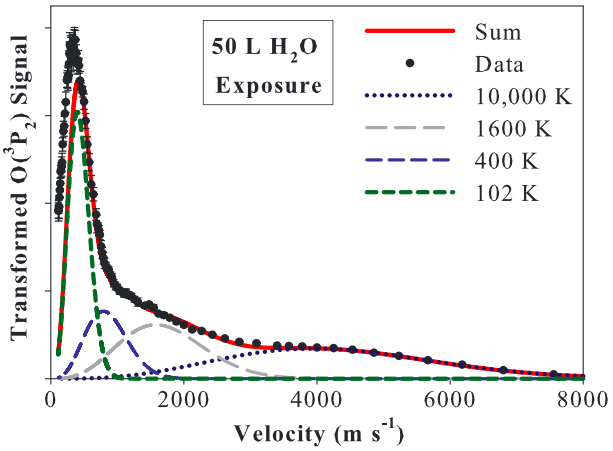

Figure 5. Velocity distribution for $O(^3P_2)$ produced by 157 nm irradiation of 50 L ASW on the lunar slab at 102 K. Four Maxwell-Boltzmann components sum to fit the data with the exception of the diffusion component.

1800 K and 400 K components continued to increase until ~ 7×10^{18} photons cm^{-2}, and the thermal component decreased much more quickly than the other components. The TOF spectra depicted in Figure 10, along with several others, were fit with four Maxwell-Boltzmann components. The integrated areas of these components and the remaining area of the diffusion component were plotted as a function of total irradiation. Figure 11 summarizes the effects of total irradiation on each TOF component individually. Effective $O(^3P_2)$ depletion cross sections (σ) for each component were determined by fitting the decreasing TOF component areas with exponential equations of the form $y = Ae^{-\sigma x}$, where x has units of photons cm^{-2} and σ is the cross section for $O(^3P_2)$ depletion. These component-specific cross sections are listed in Table 3, along with an overall cross section obtained by fitting the decreasing total yield with an exponential equation. Component and overall cross sections were also obtained for 1 L exposure, and these are listed in Table 3 as well. The overall cross section from 0.1 L ASW on the lunar slab was found to be 4.9×10^{-20} cm^2. Component cross sections for the 0.1 L ASW were not calculated because the shape of the distribution did not change significantly as signal decreased. For 50 L ASW, $O(^3P_2)$ signal did not decrease within the experimental time frame, so no cross sections could be computed.

4. Discussion

4.1. Mechanisms of $O(^3P_J)$ Formation

The mechanisms of $O(^3P_J)$ formation due to 157 nm irradiation of ASW on the lunar slab are molecular elimination following ion-electron recombination, recombination of hydroxyl radicals, and photodissociation of adsorbed OH. Specifically, $O(^3P_J)$ may be formed by molecular elimination if triplet water is produced by ionization and subsequent ion-electron recombination, according to reactions (3)–(5).

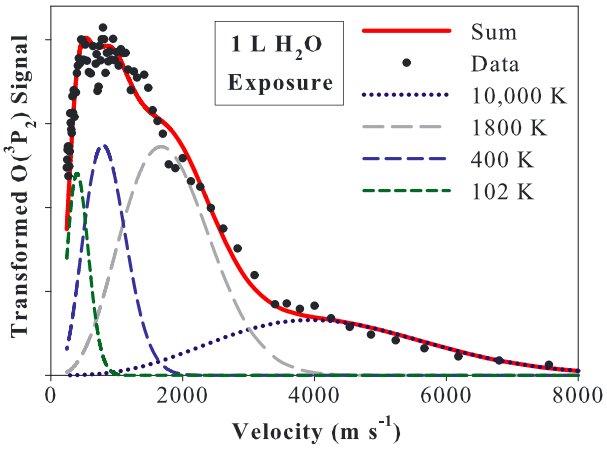

Figure 6. Velocity distribution for $O(^3P_2)$ produced by 157 nm irradiation of 1 L ASW on the lunar slab at 102 K. Four Maxwell-Boltzmann components sum to fit the data.

$$H_2O + h\nu \rightarrow H_2O^+ + e^- \quad (3)$$

$$H_2O^+ + e^- \rightarrow H_2O^*(^3B_1) \quad (4)$$

$$H_2O^*(^3B_1) \rightarrow H_2(^1\Sigma_g^+) + O(^3P). \quad (5)$$

The 400 K component has substantial signal from freshly dosed water, as indicated by the "Background" rows of Table 1, and the translational energy of the 400 K component (70 meV) is similar to the energy of $O(^3P_2)$ produced by molecular elimination in D_2O ice subjected to electron irradiation (60 meV) [*Kimmel and Orlando*, 1995]. Therefore, the molecular elimination mechanism may be responsible for the 400 K component.

©2014. American Geophysical Union. All Rights Reserved.

Table 1. Relative Yields for Each TOF Spectrum and Percentages of TOF Areas Attributed to Each Maxwell-Boltzmann or Diffusion Component

	Rel. Yield	10,000 K	1,800 K	400 K	102 K	Diffusion
			J = 0			
Background	0.34	0	31.8	68.2	0	
0.1 L	1.0	14.3	34.5	51.2	0	
1 L	1.8	13.9	32.8	41.1	12.2	
5 L	2.4	17.6	32.0	36.6	13.8	
50 L	3.9	21.7	22.6	28.7	27.0	
			J = 1			
Background	0.83	0	35.2	64.8	0	
0.1 L	2.4	11.5	33.4	42.4	12.7	
1 L	4.4	16.7	34.9	30.5	17.9	
5 L	6.6	17.4	29.2	28.6	24.8	
50 L	14.0	21.7	18.2	23.8	27.3	9
			J = 2			
Background	3.1	0	19.4	69.8	10.8	
0.1 L	8.6	9.6	26.9	43.9	19.6	
1 L	12.3	5.9	24.0	18.4	28.7	23.0
5 L	22.4	5.8	7.2	9.6	33.9	43.5
50 L	52.7	6.1	5.8	10.5	26.9	50.7
50 L at 140 K	37.2	1.0	3.3	6.1	27.0	62.6

$O(^3P_J)$ may also be formed by hydroxyl recombination reactions following photodissociation of H_2O. Four different exothermic recombination reactions of hydroxyls are possible:

$$OH(i) + OH(i) \rightarrow H_2O(i) + O(^3P) \quad (6)$$

$$OH(i) + OH(i) \rightarrow H_2O(ads) + O(^3P) \quad (7)$$

$$OH(i) + OH(ads) \rightarrow H_2O(i) + O(^3P) \quad (8)$$

$$OH(i) + OH(ads) \rightarrow H_2O(ads) + O(^3P), \quad (9)$$

where "i" stands for the vacuum/ASW interface and "ads" stands for adsorbed [*Hama et al.*, 2009]. Enthalpies for these reactions are $\Delta_r H(6) = -0.73$ eV, $\Delta_r H(7) = -1.19$ eV, $\Delta_r H(8) = -0.17$ eV, and $\Delta_r H(9) = -0.63$ eV [*Hama et al.*, 2009]. Reactions (6) and (9) are close in energy and may both contribute to the observed "1800 K" component, which was actually allowed to vary between 1600 and 2000 K in order to get the best fit for each TOF spectrum. The 400 K component may arise in part from reaction (8). As shown in Figure 9, for 0.1 L ASW on the lunar slab, this 400 K component increases more than the 1800 K component with increasing irradiation, causing the overall peak position to shift to longer times with increasing irradiation. Reaction (8) involves an adsorbed hydroxyl group, so a buildup of hydroxyls due to increasing irradiation enhances the $O(^3P)$ signal due to this reaction.

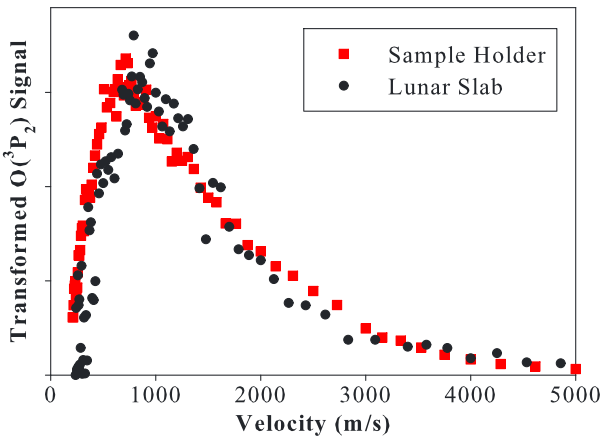

Figure 7. $O(^3P_2)$ velocity distributions produced by 157 nm irradiation of a thin layer of ASW background deposited on the partially oxidized copper sample holder (82 K) and on the impact melt breccia (102 K).

In our previous work [*DeSimone and Orlando*, 2014b], reaction (7) was not assigned to any particular Maxwell-Boltzmann component. If the released energy from that reaction (1.19 eV) goes entirely into kinetic energy and momentum conservation leads to a

©2014. American Geophysical Union. All Rights Reserved.

Table 2. Boltzmann Temperatures (K) of the Spin-Orbit Levels for Each TOF Component and Overall (Based on Total TOF Yields)

	10,000 K	1,800 K	400 K	102 K	Diffusion	Overall
Background	N/A	2,334	446	N/A		470
0.1 L	1247	865	631	102		513
1 L	Negative	9,371	Negative	270		848
5 L	Negative	Negative	Negative	216		472
50 L	Negative	Negative	Negative	321	89	319

division of this kinetic energy among the products in a ratio determined by their masses, an upper bound of 3660 K can be calculated for the translational temperature of $O(^3P)$ produced by reaction (7). Consequently, it is probably not responsible for the 10,000 K component.

In reaction (7), the water molecule adsorbs, and excess internal energy is lost to the bulk. Therefore, reaction (7) is more likely to happen in a pore than on the surface, as the water molecule will have more opportunity to lose its excess energy and adsorb when formed in a pore. However, $O(^3P)$ formed within a pore also has a greater chance of making contact with the surface before being detected. These $O(^3P)$ atoms lose most of their kinetic energy and appear as part of the thermal and diffusion components.

Photodissociation of adsorbed hydroxyls, according to reaction (10), is the most likely mechanism for forming the 10,000 K component:

$$\mathrm{OH(ads)} + \mathrm{hv(157\ nm)} \rightarrow \mathrm{H(i\ or\ ads)} + \mathrm{O}\left(^3\mathrm{P}\right). \quad (10)$$

Because unintentional background dosing is constant, it mimics the pulsed dosing of fresh water in the similar study of $O(^3P)$ formation in 1500 L ASW [*Hama et al.*, 2009]. Consequently, there is no 10,000 K component in the background TOF spectra, as this component requires hydroxyl groups to be available for photodissociation [*DeSimone and Orlando*, 2014b]. While dissociative adsorption on these lunar slabs cannot be ruled out at higher temperatures, the lack of a 10,000 K component at low coverages of freshly dosed water suggests that the formation of hydroxyl groups requires irradiation at low temperatures.

When $O(^3P)$ is formed with an initial trajectory toward the surface, it may equilibrate with the surface and emerge with a translational temperature equal to the surface temperature. Slower-than-thermal signal is also observed because diffusion out of pores in the lunar slabs can take up to 20 μs. This diffusion signal is enhanced by heating, as seen in the last row of Table 1. The diffusion component is much larger on the lunar slab than on the copper sample holder due to the greater porosity of the lunar slab [*DeSimone and Orlando*, 2014b].

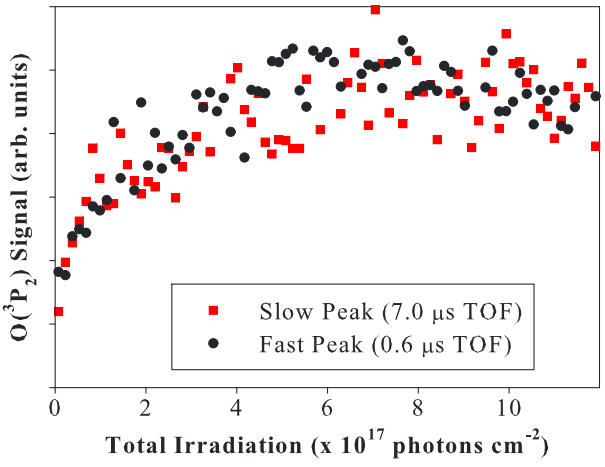

Figure 8. $O(^3P_2)$ signal produced by 157 nm irradiation of 50 L ASW on the lunar slab at TOF = 0.6 μs (red squares) and 7.0 μs (black circles) as a function of total irradiation.

4.2. Effect of Irradiation on ASW Adsorbed on Lunar Slab

As shown in Figure 11, irradiation of 5 L ASW with ~5×10^{18} photons cm^{-2} was required before $O(^3P_2)$ signal stopped increasing and began to decrease. For 1 L ASW, only ~1×10^{18} photons cm^{-2} resulted in maximum signal. In the 1−5 L exposure range, it seems that the number of photons required to completely hydroxylate the surface is proportional to the amount of water dosed. It is probable that 1 L exposure is much less than one full layer of coverage. Water may form three-dimensional clusters when adsorbed on the impact melt breccia, as the surface is expected to be mostly glassy and hydrophobic. However, it is also a multiphase material with a multitude of defects that may be amenable to water or

©2014. American Geophysical Union. All Rights Reserved.

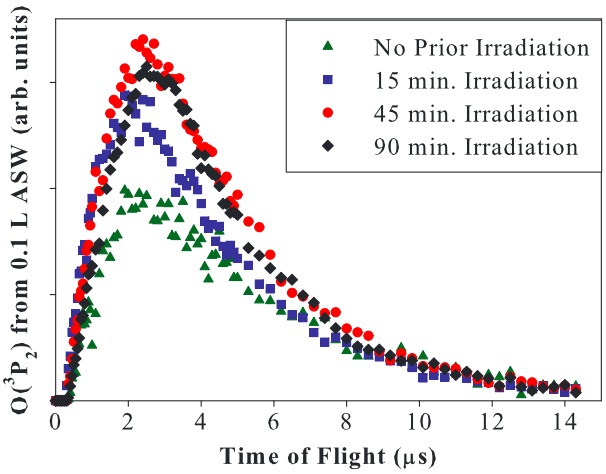

Figure 9. $O(^3P_2)$ TOF spectra from 0.1 L ASW on the lunar slab after 0, 15, 45, and 90 min of 157 nm irradiation.

hydroxyl chemisorption [*Poston et al.*, 2013]. Perhaps, once a hydroxyl group is produced, it migrates away from the ASW cluster until it finds a chemisorption site on the substrate. This migration continues to occur until the ASW clusters are broken up into individually adsorbed hydroxyl groups or H_2O_2. Because the clusters are five times larger for five times the exposure, this process requires five times as many photons for 5 L as for 1 L.

According to molecular dynamics simulations, OH and H radicals produced in the top three layers of ice can diffuse up to 60 and 70 Å along the surface, respectively [*Andersson and van Dishoeck*, 2008]. Migrating hydroxyl groups either recombine to form H_2O_2 or eventually lose enough energy to become trapped as individually adsorbed hydroxyl groups. Subsequent photodissociation of H_2O_2 may release energetic hydroxyl groups that can also diffuse along the surface or desorb [*Hama et al.*, 2009]. Therefore, the spreading out of water clusters can occur through OH (and H) migration following photodissociation.

In contrast to the long irradiation time required to reach maximum $O(^3P_2)$ signal at 5 L exposure, 50 L ASW only requires 5×10^{17} photons cm^{-2} to reach maximum signal. At 50 L exposure, the surface should be completely covered, so the cluster scenario no longer applies. Photoirradiation dissociates the maximum number of water molecules per cm^2, and the top layer is most quickly hydroxylated.

4.3. Implications for Oxygen in the Lunar Atmosphere

The measured $O(^3P_2)$ depletion cross sections in Table 3 are lower than the total water removal cross sections from the same lunar substrate, which are reported in the companion paper [*DeSimone and Orlando*, 2014a]. Also in contrast to water removal cross sections, $O(^3P_2)$ depletion cross sections do not always increase as coverage decreases. The most extreme difference can be seen at 0.1 L, where the cross section for water depletion ($\sim 7 \times 10^{-19}$ cm^2) is more than an order of magnitude higher than that for $O(^3P_2)$ depletion. However, these cross sections are measured at different times. The H_2O removal cross section is measured immediately following the start of irradiation, while the $O(^3P_2)$ removal cross section is measured after $O(^3P_2)$ signal reaches its maximum. A low rate of $O(^3P_2)$ depletion could be due to hydroxyls on the surface being replaced by photodissociation of water almost as quickly as they react. Because the water removal cross section also includes losses due to photodissociation, together, the H_2O and $O(^3P_2)$ removal cross sections may indicate that photodissociation is more important at low coverages than at high coverages.

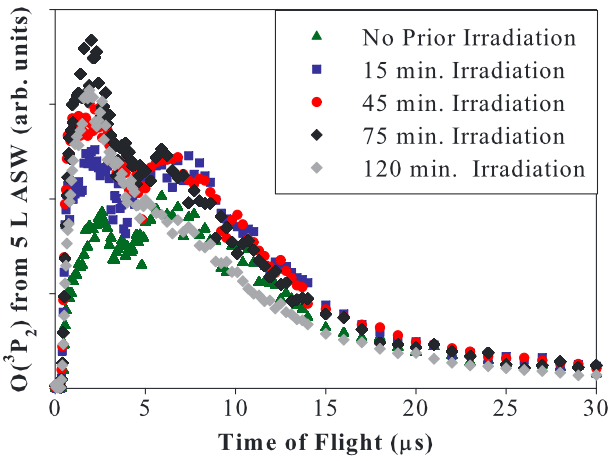

Figure 10. $O(^3P_2)$ TOF spectra from 5 L ASW on the lunar slab after 0, 15, 45, 75, and 120 min of 157 nm irradiation.

In our companion paper [*DeSimone and Orlando*, 2014a], the H_2O removal/destruction rate due to ultraviolet photons is estimated. A similar calculation can be employed to estimate the flux of $O(^3P)$ desorbing from the lunar surface due to ultraviolet photons. Goldschmidt crater will be used as an example due to its enhanced OH/H_2O signal.

©2014. American Geophysical Union. All Rights Reserved.

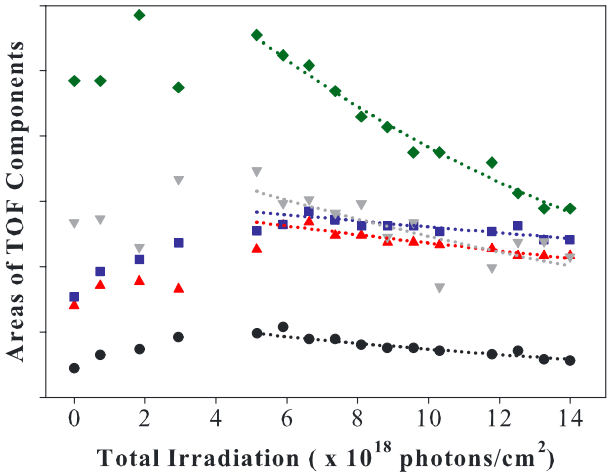

Figure 11. Integrated areas of components fitted to $O(^3P_2)$ TOF spectra for 5 L ASW on the lunar slab at 102 K. 10,000 K = black circles, 1800 K = red up triangles, 400 K = blue squares, 102 K = green diamonds, diffusion = gray down triangles. Dotted lines represent exponential fits of the form $y = Ae^{-\sigma x}$, where x has units of photons cm^{-2}.

The same assumptions will be made as in our complementary work [*DeSimone and Orlando*, 2014a]. The solar photon flux, F_{ph}, at the lunar surface above 8 eV is 10^{12} photons $cm^{-2}\,s^{-1}$ [*Yakshinskiy and Madey*, 1999]. In Goldschmidt crater, the top 0.66 nm (about 1 ML) of lunar regolith contains about 4.4×10^{14} water-equivalent hydrogens per cm^2 [*Lawrence et al.*, 2011]. Since we believe that our cross section was obtained after irradiation significantly hydroxylated the surface, many of these water-equivalent hydrogens may actually be part of OH groups, but both H_2O and OH are required for recombination reactions. If we assume that an equal number of OH groups and H_2O molecules are present, the water-equivalent hydrogens are part of 1.5×10^{14} OH groups and H_2O molecules per cm^2. Since 1×10^{15} molecules cm^{-2} corresponds to 1 L exposure when the sticking probability equals one, 1.5×10^{14} molecules cm^{-2} roughly corresponds to 0.15 L. Since Goldschmidt crater has experienced many impact events, we choose the overall $O(^3P)$ depletion cross section from 0.1 L H_2O on the impact melt breccia, $\sigma = 4.9 \times 10^{-20}$ cm^2. The flux of $O(^3P)$, $\Phi_{O(3P)}$, from the sunlit parts of Goldschmidt crater due to solar photons is then

$$\Phi_{O(3P)} = F_{ph}\sigma\,\theta \approx 7.4 \times 10^6 \text{atoms cm}^{-2}\text{s}^{-1}, \quad (11)$$

where θ is coverage in units of molecules cm^{-2}.

In order to calculate the surface density in cm^{-3}, $\Phi_{O(3P)}$ should be divided by the effective velocity. Using the total fit shown in Figure 6 (extending down to nearly zero yields at 68 m/s), each velocity was weighted according to its yield, and a total $O(^3P_J)$ density of 68 cm^{-3} was determined. This result is lower than all reported upper bounds for the surface density of oxygen. The Apollo 17 UV spectrometer found the surface density of oxygen to have an upper limit of ~80 cm^{-3} [*Fastie et al.*, 1973], and a more extensive analysis updated this limit to ~500 cm^{-3} [*Feldman and Morrison*, 1991].

The recent pickup ion measurements of *Halekas et al.* [2013] resulted in an upper limit of 12,000 cm^{-3} for the density of oxygen atoms in the lunar atmosphere. Our estimated density of 68 cm^{-3} only represents $O(^3P_J)$ atoms produced by photoirradiation, but $O(^1D)$ may be produced directly by photodissociation of H_2O and may contribute to the observed mass-16 signal in the pickup ion measurements. Many other mechanisms of seeding the atmosphere with oxygen were also considered by *Halekas et al.* [2013], since the pickup ions were observed after the Moon had been sitting in the magnetosheath's plasma for 30 h. Furthermore, *Halekas et al.* [2013] noted that the surprisingly large mass-16 signal could be partly due to CH_4 in the lunar atmosphere, and it could have contributions from mass-17 OH as well. Our results imply that photodissociation of water on the lunar surface cannot account for the large mass-16 signal observed by *Halekas et al.* [2013].

Table 3. Cross Sections (cm^2) for $O(^3P_2)$ Depletion by 157 nm Irradiation of 5 and 1 L ASW on the Impact Melt Breccia

	10,000 K	1,800 K	400 K	102 K	Diffusion	Overall
5 L	5.9×10^{-20}	2.6×10^{-20}	1.7×10^{-20}	7.5×10^{-20}	5.1×10^{-20}	4.6×10^{-20}
1 L	9.6×10^{-20}	6.6×10^{-20}	4.1×10^{-20}	1.5×10^{-19}	N/A	6.6×10^{-20}

©2014. American Geophysical Union. All Rights Reserved.

5. Conclusion

Photodissociation of water deposited on an impact melt breccia collected during Apollo 16 was studied by measuring $O(^3P_{J=2,1,0})$ photoproducts detected with resonance-enhanced multiphoton ionization. For each spin-orbit state, the oxygen atom time-of-flight spectrum was measured as a function of H_2O exposure and 157 nm irradiation time, and four Maxwell-Boltzmann distributions with translational temperatures of 10,000 K, 1800 K, 400 K, and 102 K were required to fit the data. The most likely formation mechanisms are molecular elimination following ion-electron recombination, secondary recombination of hydroxyl radicals, and photodissociation of adsorbed hydroxyls. Evidence for diffusion out of pores in the lunar substrate was found for H_2O exposures of at least 1 L. The irradiation time required to reach maximum oxygen signal suggests that water clusters into islands when adsorbing on the lunar impact melt breccia. After enough irradiation for the oxygen yield to reach its maximum, the slowly decreasing signal was fit with an exponential curve to obtain a cross section that represents the rate of surface hydroxyl depletion. For 0.1, 1, and 5 L H_2O exposure, respectively, the measured $O(^3P)$ depletion cross sections were 4.9×10^{-20}, 6.6×10^{-20}, and 4.6×10^{-20} cm^2. The estimated lunar surface density of oxygen atoms due to photodissociation of water is too low to explain the unexpectedly large mass-16 signal in recent pickup ion measurements.

Acknowledgments
This work was supported by the NASA LASER program grant number NNX11AP13G. The authors also thank Gregory Grieves for useful discussions.

References

Andersson, S., and E. F. van Dishoeck (2008), Photodesorption of water ice A molecular dynamics study, *Astron. Astrophys.*, *491*(3), 907–916, doi:10.1051/0004-6361:200810374.

Andersson, S., C. Arasa, A. Yabushita, M. Yokoyama, T. Hama, M. Kawasaki, C. M. Western, and M. N. R. Ashfold (2011), A theoretical and experimental study on translational and internal energies of H2O and OH from the 157 nm irradiation of amorphous solid water at 90 K, *Phys. Chem. Chem. Phys.*, *13*(35), 15,810–15,820, doi:10.1039/c1cp21138b.

Cassidy, T., P. Coll, F. Raulin, R. W. Carlson, R. E. Johnson, M. J. Loeffler, K. P. Hand, and R. A. Baragiola (2010), Radiolysis and photolysis of icy satellite surfaces: Experiments and theory, *Space Sci. Rev.*, *153*(1-4), 299–315, doi:10.1007/s11214-009-9625-3.

Clark, R. N. (2009), Detection of adsorbed water and hydroxyl on the Moon, *Science*, *326*(5952), 562–564, doi:10.1126/science.1178105.

DeSimone, A. J., and T. M. Orlando (2014a), Mechanisms and cross sections for water desorption from a lunar impact melt breccia, companion paper in, *J. Geophys. Res. Planets*, doi:10.1002/2013JE004599, in press.

DeSimone, A. J., and T. M. Orlando (2014b), $O(^3P_J)$ formation and desorption by 157-nm photoirradiation of amorphous solid water, *J. Chem. Phys.*, *140*(9), 094,702.

DeSimone, A. J., V. D. Crowell, C. D. Sherrill, and T. M. Orlando (2013), Mechanisms of H_2O desorption from amorphous solid water by 157-nm irradiation: An experimental and theoretical study, *J. Chem. Phys.*, *139*(16), 164,702.

Fastie, W. G., P. D. Feldman, R. C. Henry, H. W. Moos, C. A. Barth, G. E. Thomas, and T. M. Donahue (1973), Search for far ultraviolet emissions from lunar atmosphere, *Science*, *182*(4113), 710–711, doi:10.1126/science.182.4113.710.

Feldman, P. D., and D. Morrison (1991), The Apollo 17 ultraviolet spectrometer - Lunar atmosphere measurements revisited, *Geophys. Res. Lett.*, *18*(11), 2105–2108, doi:10.1029/91gl01998.

Halekas, J. S., A. R. Poppe, G. T. Delory, M. Sarantos, and J. P. McFadden (2013), Using ARTEMIS pickup ion observations to place constraints on the lunar atmosphere, *J. Geophys. Res. Planets*, *118*, 81–88, doi:10.1029/2012je004292.

Hama, T., A. Yabushita, M. Yokoyama, M. Kawasaki, and N. Watanabe (2009), Formation mechanisms of oxygen atoms in the O(P-3(J)) state from the 157 nm photoirradiation of amorphous water ice at 90 K, *J. Chem. Phys.*, *131*(11), 114511, doi:10.1063/1.3194797.

Hama, T., M. Yokoyama, A. Yabushita, M. Kawasaki, S. Andersson, C. M. Western, M. N. R. Ashfold, R. N. Dixon, and N. Watanabe (2010), A desorption mechanism of water following vacuum-ultraviolet irradiation on amorphous solid water at 90 K, *J. Chem. Phys.*, *132*(16), 164,508, doi:10.1063/1.3386577.

Hibbitts, C. A., G. A. Grieves, M. J. Poston, M. D. Dyar, A. B. Alexandrov, M. A. Johnson, and T. M. Orlando (2011), Thermal stability of water and hydroxyl on the surface of the Moon from temperature-programmed desorption measurements of lunar analog materials, *Icarus*, *213*(1), 64–72, doi:10.1016/j.icarus.2011.02.015.

Kimmel, G. A., and T. M. Orlando (1995), Low-energy (5–120-eV) electron-stimulated dissociation of amorphous D2O ICE - D(S-2), O(P-3(2,1,0), and O(D-1(2)) yields and velocity distributions, *Phys. Rev. Lett.*, *75*(13), 2606–2609, doi:10.1103/PhysRevLett.75.2606.

Lawrence, D. J., D. M. Hurley, W. C. Feldman, R. C. Elphic, S. Maurice, R. S. Miller, and T. H. Prettyman (2011), Sensitivity of orbital neutron measurements to the thickness and abundance of surficial lunar water, *J. Geophys. Res.*, *116*, E01002, doi:10.1029/2010je003678.

Matsumi, Y., N. Shafer, K. Tonokura, M. Kawasaki, Y. L. Huang, and R. J. Gordon (1991), Doppler profiles and fine-structure branching ratios of O(P-3(J)) from photodissociation of carbon-dioxide at 157 nm, *J. Chem. Phys.*, *95*(10), 7311–7316, doi:10.1063/1.461408.

Nishi, N., H. Shinohara, and T. Okuyama (1984), Photodetachment, photodissociation, and photochemistry of surface molecules of icy solids containing NH_3 and pure H_2O ICES, *J. Chem. Phys.*, *80*(8), 3898–3910, doi:10.1063/1.447172.

Pieters, C. M., et al. (2009), Character and spatial distribution of OH/H_2O on the surface of the Moon seen by M-3 on Chandrayaan-1, *Science*, *326*(5952), 568–572, doi:10.1126/science.1178658.

Poston, M. J., G. A. Grieves, A. B. Aleksandrov, C. A. Hibbitts, M. D. Dyar, and T. M. Orlando (2013), Water interactions with micronized lunar surrogates JSC-1A and albite under ultra-high vacuum with application to lunar observations, *J. Geophys. Res. Planets*, *118*, 105–115, doi:10.1029/2012je004283.

Sunshine, J. M., T. L. Farnham, L. M. Feaga, O. Groussin, F. Merlin, R. E. Milliken, and M. F. A'Hearn (2009), Temporal and spatial variability of lunar hydration as observed by the deep impact spacecraft, *Science*, *326*(5952), 565–568, doi:10.1126/science.1179788.

Thiel, P. A., and T. E. Madey (1987), The interaction of water with solid-surfaces: Fundamental aspects, *Surf. Sci. Rep.*, *7*(6-8), 211–385, doi:10.1016/0167-5729(87)90001-x.

©2014. American Geophysical Union. All Rights Reserved.

Yabushita, A., T. Hama, D. Iida, and M. Kawasaki (2008), Hydrogen peroxide formation following the vacuum ultraviolet photodissociation of water ice films at 90 K, *J. Chem. Phys.*, *129*(1), 014709, doi:10.1063/1.2950093.

Yabushita, A., T. Hama, M. Yokoyama, M. Kawasaki, S. Andersson, R. N. Dixon, M. N. R. Ashfold, and N. Watanabe (2009), Translational and rotational energy measurements of photodesorbed water molecules in their vibrational ground state from amorphous solid water, *Astrophys. J. Lett.*, *699*(2), L80–L83, doi:10.1088/0004-637x/699/2/l80.

Yakshinskiy, B. V., and T. E. Madey (1999), Photon-stimulated desorption as a substantial source of sodium in the lunar atmosphere, *Nature*, *400*(6745), 642–644.

Zimmermann, F. M., and W. Ho (1995), State-resolved studies of photochemical dynamics at surfaces, *Surf. Sci. Rep.*, *22*(4-6), 127–247, doi:10.1016/0167-5729(96)80001-X.

©2014. American Geophysical Union. All Rights Reserved.